

Molecular Dynamics Simulation of a GM3 Ganglioside Bilayer

Marcello Sega and Renzo Vallauri*

INFM and Department of Physics, University of Trento, Via Sommarive 14, I-38050 Povo (Trento), Italy

Paola Brocca

Department of Chemistry, Biochemistry and Biotechnologies for Medicine, University of Milan, via F.lli Cervi 93, I-20090 Segrate (MI), Italy, and INFM

Simone Melchionna

INFM and Department of Physics, University of Rome "La Sapienza", P.le A. Moro 2, I-00185 Rome, Italy

Received: July 13, 2004; In Final Form: October 7, 2004

A first molecular dynamics simulation of a fully hydrated GM3 ganglioside bilayer is presented. Several properties characterizing the membrane structure and surrounding water are evaluated and compared to known data related to phospholipids. Our results are in good agreement with experimental small-angle X-ray scattering data. Overall, the simulated bilayer shows very long relaxation times such that a full equilibration is attained in about 30 ns. The long equilibration time is due to the slow relaxation of the torsional angle at the level of the galactose–sialic acid linkage. Once equilibrated, GM3 exhibits a good packing of the hydrophilic moieties, due to preferential alignment of its longitudinal axis along the bilayer normal, and a high degree of disorder in the tail region. The ionic nature of the hydrophilic heads manifests itself in a slow decay of the water orientational order parameter.

1. Introduction

In recent years gangliosides have attracted the attention of many research groups, due to their importance as biological constituents.¹ Gangliosides are found in the plasma membrane of eukaryotic cells and are particularly abundant in the nervous system. They are believed to play an active role in the formation and function of lipid rafts² and in the membrane-mediated interactions of the cell with its environment.³ Gangliosides are a broad class of amphiphiles whose hydrophilic moiety is composed by a variable number of saccharidic rings and sialic acid residues, carrying thus a net negative charge. Gangliosides in solution form different aggregates with a very rich phase diagram and consequently have been extensively studied by various experimental techniques such as NMR, calorimetry, and neutron, light, and X-ray scattering (see, for example, refs 4–6).

Three main features distinguish gangliosides from phospholipids, namely the large steric contribution associated with the hydrophilic headgroup, the ionic nature of this unit, and the presence of ceramide as the hydrophobic portion. The combination of these contributions determines the peculiar packing of the molecules within the aggregate and, therefore, its global geometry. As a matter of fact, gangliosides aggregate in a variety of shapes and dimensions, namely micelles, vesicles, and bilayers. Two common variants of gangliosides, which illustrate this variety, are GM3 (depicted in Figure 1) and GM1, bearing respectively three and five sugar rings. The former aggregates into vesicles and bilayers, while the latter forms micelles.⁷ However, GM3 forms vesicles in solution spontaneously,⁸ suggesting that, when compared to the case of phospholipids, the steric hindrance of the hydrophilic moiety lowers the bending

energy of the bilayer. Generally speaking, the kind of aggregate formed by a surfactant can be characterized in simple, geometrical terms by the packing parameter $P = v/a_0l$, where a_0 is the area per headgroup at the interface, v is the volume per molecule, and l is the length of the hydrocarbon chain. Different values of P give rise to spherical ($P \approx 1/3$) or elongated micelles ($1/3 < P < 1/2$) or vesicles and bilayers ($P > 1/2$), and therefore, GM3 should fall into this latter class of amphiphiles.

Due to the difficulties in treating such complex systems, computer simulation has only been employed sporadically in the study of gangliosides. To the best of our knowledge, computer simulation has only been used to investigate the single molecule behavior of GM3 and GM1 (see, for example, refs 4 and 9). In these studies the solvent has been taken into account mostly in an effective way by means of appropriate model interactions between the head units. Overall, these preliminary studies have found good agreement with available NMR data, in particular as regarding the orientation of the head rings. Molecular dynamics simulations of a ganglioside aggregate have never been attempted before.

In a long term project aiming at the characterization of ganglioside aggregates, we have tackled the study of a GM3 bilayer. In this paper we present the results of the first molecular dynamic simulation of a fully hydrated bilayer made of 128 GM3 molecules in the liquid-crystalline phase. Our results are compared with available experimental data, as well as with analogous data obtained for the more often investigated phospholipids such as dipalmitoylphosphatidylcholine (DPPC) and dimyristoylphosphatidylcholine (DMPC).^{10,11}

2. Model and Simulation Details

2.1. The Force Field. The GM3 molecules were modeled using a modified version of the GROMACS^{12,13} force field,

* Electronic address: vallauri@science.unitn.it.

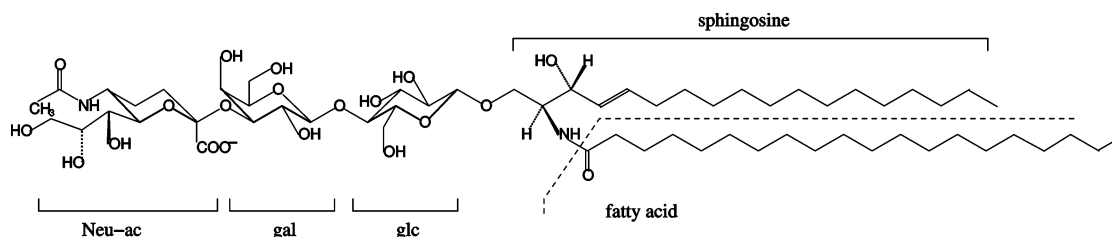


Figure 1. Chemical structure of the GM3 molecule. The constituent subunits of the headgroup are labeled as glc (glucose), gal (galactose), and Neu-ac (sialic acid). The two constituents of the ceramide, sphingosine and the fatty acid, are also highlighted.

which in turn is essentially the GROMOS87¹⁴ one with some minor changes. The simulation is performed at atomistic detail, treating the aliphatic groups, CH, CH₂, and CH₃, as united atoms. The resulting total number of atoms explicitly representing GM3 amounts to 97. The Ryckaert–Bellemans¹⁵ dihedral potential was used to model the torsional angles in the lipid tails, whereas improper dihedral potentials were used to mimic the chiral centers of the GM3 molecule, as well as the planar double bond connecting unsaturated carbon atoms in the sphingosine. Partial charges were assigned by using the PRODRG program.¹⁶

Since it has been reported^{17,18} that the GROMOS87 force field needs to be improved in its carbohydrate part to better adhere with experimental data, some modifications were applied to the carbohydrate rings. We have adopted the method of Spieser¹⁹ to account for the rigidity of the sugar rings and to correctly reproduce the exoanomeric torsion angles. Moreover, to better describe the density of the lipid part of the bilayer, we have employed the Lennard-Jones parameters suggested by Berger¹⁰ for pentadecane, as already adopted in many simulations of lipid bilayers. This choice appears to be the most reasonable, even if in the present case the lipid tails are longer than in phospholipids. Water has been modeled by the single point charge model (SPC), an accurate choice for reproducing interfacial properties, as pointed out in ref 20.

2.2. Starting Configuration and Simulation Details. The starting configuration of the hydrated bilayer was constructed by applying the following protocol. Starting from the configuration of a single GM3 molecule in effective water (dielectric permittivity $\epsilon_r = 80$), we brought the structure to a configuration of minimum energy by simulated annealing, letting temperature drop 10 times from 6000 to 0 K over a period of 100 ps. The GM3 molecule was finally rotated to have its principal axis aligned along the *z* direction. Two monolayers were then assembled by putting together copies of the GM3 energetically minimized structure on a 8×8 square lattice, with a lattice spacing of 1 nm. To add static disorder, molecules were then randomly rotated around the *z* axis. These operations resulted in a distance larger than 0.1 nm between atoms belonging to different GM3 molecules. The two monolayers were assembled to form a bilayer composed by 128 GM3 molecules. To avoid overlaps between atoms in the tail region, introduced by the operation of joining the two monolayers together, the system was energy-minimized with the conjugate gradient method. To neutralize the total charge, 128 Na⁺ counterions were placed within a simulation box of the *z*-edge of 11.2 nm at random positions, at a distance larger than 0.25 nm from any atom of the GM3 molecules. A short run of 50 ps at constant volume and constant temperature of 600 K was then performed, keeping the GM3 molecules fixed in space, to allow the counterions to partially condensate on the negative charges of GM3.

At this stage, the surface density of the membrane was very low. Therefore, we have performed a simulation run to relax the *x* and *y* box vectors, while keeping the *z* box vector fixed

as well as the simulation box angles at 90°. In this way, the GM3 molecules rapidly packed without destroying the membrane structure. The final box vectors were equal to 6.7, 6.6, and 11.2 nm in the *x*, *y*, and *z* directions, respectively. Subsequently, water molecules were added in the simulation box, taking their positions from a configuration of equilibrated SPC water and deleting molecules with a distance smaller than the sum of the Van der Waals radii of the water atoms and any other atom belonging to GM3 or counterions. The final number of added water molecules amounts to 6724 units. The choice of the water layer size is a compromise between the need to minimize spurious interactions between periodic images and the computational effort needed to perform the simulation. Since the procedure adopted to add water molecules is based only on geometric considerations, the obtained system is energetically unfavored. Therefore, to further relax the system, a short run of 50 ps at the constant temperature of 333 K and at constant volume was performed before starting the equilibration run.

All simulations were performed at constant pressure, temperature, and number of atoms using the GROMACS molecular dynamics package.^{12,13} It is crucial to compute electrostatics without truncating the interaction, since it has been shown that, in the simulation of nonionic amphiphiles, important unphysical effects arise when truncation is employed.²¹ The case of GM3, which is an ionic amphiphile, is even more problematic, since, as it will be shown, the electric field is only partially screened by the counterions and therefore is long ranged. Electrostatics was thus treated using the Ewald summation method in the Smooth Particle Mesh Ewald implementation,²² with a mesh spacing of 0.12 nm and a spline order of 4.

A cutoff of 0.9 nm was applied for both the Lennard-Jones interaction and short-range contribution to the Ewald sum. All bond lengths were constrained, using the SHAKE algorithm²³ in its implementation named SETTLE²⁴ for water and LINCS²⁵ for GM3. The time step of integration was set to 2 fs, exhibiting excellent energy conservation when tested in the microcanonical ensemble.

Both temperature and pressure were kept constant at 333 K and 1 atm, respectively, by means of the weak-coupling method of Berendsen et al.²⁶ At the chosen temperature and pressure, the GM3 bilayer is known to be well within the liquid-crystalline (*L_α*) region of the phase diagram. The time constants for the thermostat and piston were set to 0.1 and 1.0 ps, respectively. During both equilibration and production runs, we let the system volume fluctuate anisotropically, while fixing the simulation box angles at 90°. In this way, the three box edges were allowed to scale independently from each other, relaxing the internal stress tensor accordingly. Periodic boundary conditions were applied in all directions. During both equilibration and production runs, configurations were stored every 125 ps for subsequent analysis.

2.3. Equilibration. As already pointed out in the Introduction, one of the most peculiar characteristics of the GM3 molecule is that the headgroup has approximately the same longitudinal extension of the ceramide tail (≈ 1.8 nm). For the sake of

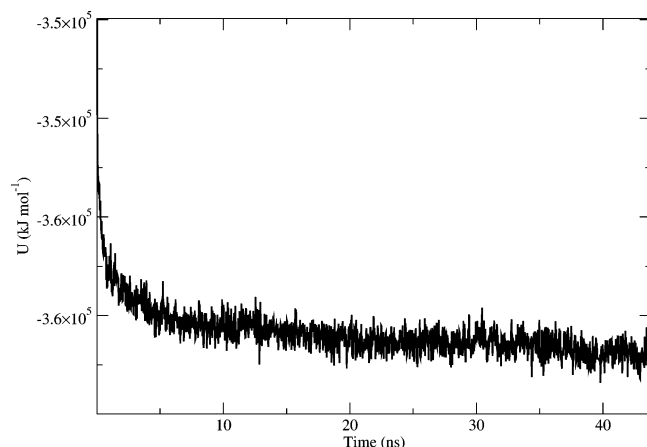


Figure 2. Time evolution of the total potential energy of the system.

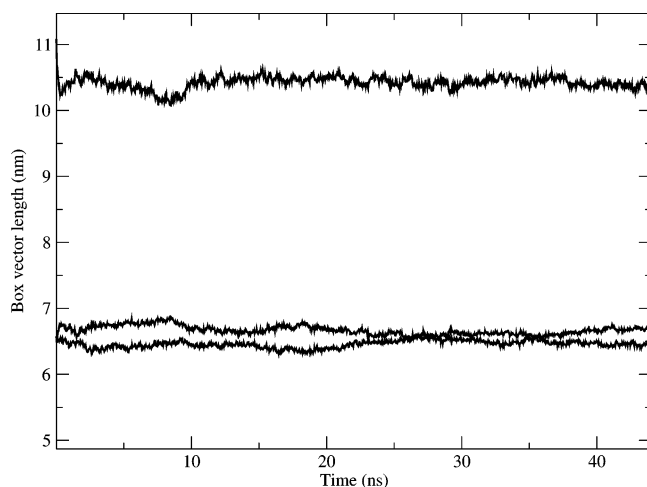


Figure 3. Time evolution of the three box vectors. From top to bottom the solid lines represent the value of the z , x , and y box vector lengths, respectively.

comparison, phospholipidic heads have approximately half the longitudinal extension of the GM3 heads, while DPPC's lipid tails have 15 carbon atoms, in contrast to GM3, which has two chains, made of 18 and 20 carbon atoms, respectively. Moreover, apart from the flexibility due to the glycosidic linkages, the sugar rings of GM3 present very rigid chemical structures. These characteristics, as well as the fact that GM3 bears a net negative charge, have posed some nontrivial problems in the equilibration stage of the simulation.

The rigidity of the components of the headgroup resulted in very long relaxation times for the system and, consequently, a long equilibration time. As illustrated in Figure 2, the total potential energy reached a stationary state in about 30 ns. This period is about 1 order of magnitude longer than that reported for phospholipids (see, for example, ref 10). On the other hand, the dimensions of the simulation box reported in Figure 3 exhibit an apparent stationary behavior for the x , y , and z components. Importantly, however, the x and y lengths of the simulation cell retain practically the same value on average.

We have identified two possible mechanisms which can contribute to the observed slow equilibration time. The first is due to the slow relaxation of the sialic acid residue, which rotates around the glycosidic linkage with galactose. The time evolution of the three dihedral angles around the glycosidic linkages, averaged over the 128 GM3 molecules, is presented in Figure 4. It is clear that the equilibration time of the dihedral angle of the sialic acid residue, the most exposed to the solvent, is by

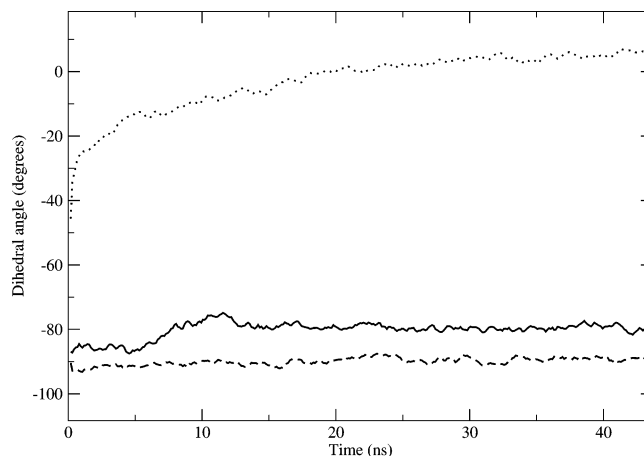


Figure 4. Time evolution of the three dihedral angles involving rotation around the ceramide–glucose (solid line), glucose–galactose (dashed line), and galactose–sialic acid (dotted line) bonds, respectively. The dihedral angles are defined by the four atoms C–O–C–O_R, where O_R is the oxygen belonging to the sugar ring. Data have been averaged over the 128 GM3 molecules.

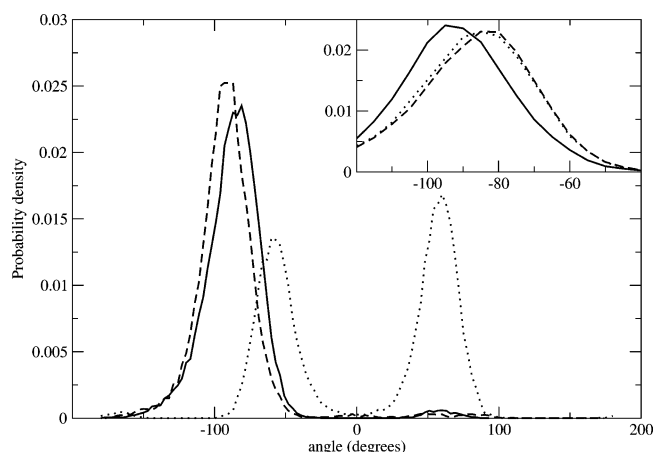


Figure 5. Normalized histograms of the torsional angles involving rotation around the ceramide–glucose (solid line), glucose–galactose (dashed line), and galactose–sialic acid (dotted line) bonds, respectively, computed as described in Figure 4. Inset: histograms for the torsional angle around the ceramide–glucose bond sampled in the time intervals (0, 10), (10, 20), and (20, 30) ns (solid, dashed, and dotted lines, respectively).

far the longest one, reaching equilibrium over the same time scale of energy, that is, after 30 ns. The equilibrium histograms of the three dihedral angles are reported in Figure 5. In the inset we report the histogram for the innermost torsional angle averaged over the time intervals (0, 10), (10, 20), and (20, 30) ns in order to observe if 30 ns is a sufficient time to reach a stationary state. The absence of a drift in the time evolution after 10 ns confirms that the histograms of the inner dihedrals can be considered equilibrium ones. It is worth noticing that the distribution of the torsional angle relative to the sialic acid residue turns out to be bimodal and nearly equally populated. This result can explain why the system spends a long time in reaching a well defined conformational state. As typical, quasi-degenerate states often produce long equilibration times, even if the energetic barrier is thermally activated. Vice versa, in the case of the other two dihedral angles, only a tiny percentage of molecules shifts to larger angles even on the longest time scale explored by the simulation. The absence of a drift in the time evolution both of the average (see Figure 4) and of the whole

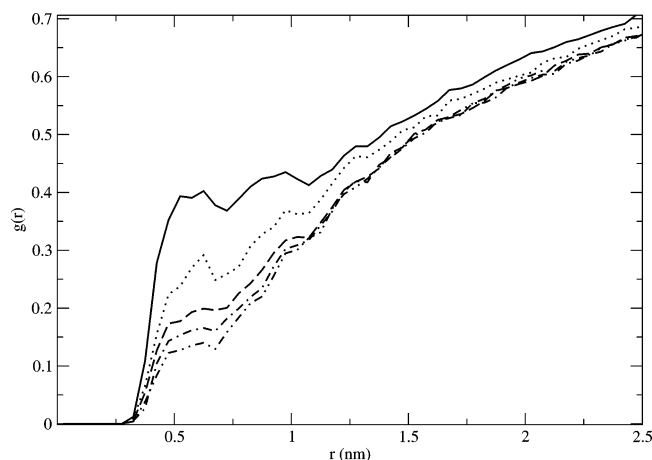


Figure 6. Radial distribution function of water oxygen around the glucose residue, averaged over 1 ns, at different times, namely at the beginning of the simulation (solid line) and at 3 ns (dotted line), 6 ns (dashed line), 12 ns (dot-dashed line), and 24 ns (dot-dot-dashed line).

distribution (see the inset of Figure 5) confirms that a definitive equilibrium has been reached after 30 ns.

The second identified contribution to the long equilibration time is the dehydration process involving the interior rings. In Figure 6 the radial distribution function of water oxygen around the center of mass of the glucose residue is shown. It appears that the number of water molecules coordinated with glucose rapidly decreases in the first 2.5 ns. As time proceeds, water is progressively expelled from the interior part of the bilayer, reducing the first peak height by a factor 2.7 with respect to the initial value, and the radial distribution function converges toward its equilibrium profile. From these results, we conclude that the system has reached equilibrium after 30 ns of the relaxation stage. In Figure 7 two snapshots of the system are reported, the first one at the beginning of the equilibration run and the second one after the equilibration has taken place,

exhibiting the high degree of conformational disorder attained by the tails over 40 ns.

3. Results and Discussion

Going into the details of the bilayer structure, in Figures 8 and 9 we report the mass density profile of the GM3 bilayer, where the contributions of the main molecular components have been separated out. The overall features are similar to those found for DPPC as well as for other phospholipids membranes, that is, a well defined hydrophobic effect, since water does not penetrate in the region where the tails are present. The mass density inside the lipid region is slightly larger for GM3 than for DMPC or DPPC, and the dry inner layer has an extension of roughly 2 nm, similarly to what was found in DPPC and DMPC bilayers (see, for example, Figure 4 in ref 10 and, Figure 1 in ref 11). These two facts suggest that the hydrophobic tails of ganglioside GM3 are more disordered than those in DMPC or DPPC. As a matter of fact, the two tails, far from being aligned with the normal to the membrane, are quite bended over and disordered. This observation can be substantiated by looking at the radial distribution functions of the CH₃ groups around the center of mass of the three sugar rings. As shown in Figure 10, the terminal groups of the hydrocarbon chains have quite high probability to be found close to the glucose residue. By integrating the distribution function up to a cutoff, one obtains the coordination number

$$N_{\alpha\beta}(R_c) = \int_0^{R_c} 4\pi\rho_\beta g_{\alpha\beta}(r)r^2 dr \quad (1)$$

where $g_{\alpha\beta}(r)$ is the radial distribution function of group β with respect to group α , ρ_β is the number density of group β , and the cutoff R_c is chosen to coincide with the first minimum of the radial distribution function. The coordination number $N_{\text{glc,CH}_3}$ of the CH₃ group with respect to the center of mass of glucose shows that about 1.5 terminal groups of the hydrocarbon chains are found in the proximity of the glucose residue.

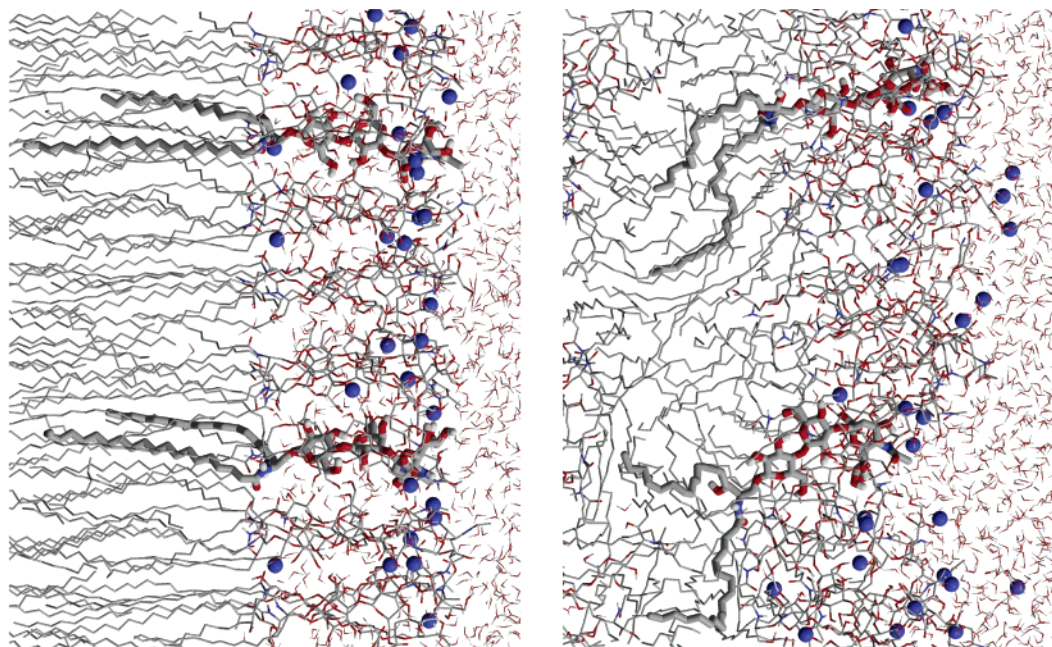


Figure 7. Snapshots of a 3 nm thick slice of the GM3 bilayer in solution. Oxygen, carbon, and hydrogen atoms have been drawn in red, gray and white, respectively. Nitrogen atoms as well as sodium counterions have been drawn in blue. Two GM3 molecules are highlighted using fat bonds. Left panel: starting configuration. Right panel: equilibrium configuration after 40 ns from the starting configuration. The drawing was made using Raster3D.²⁷

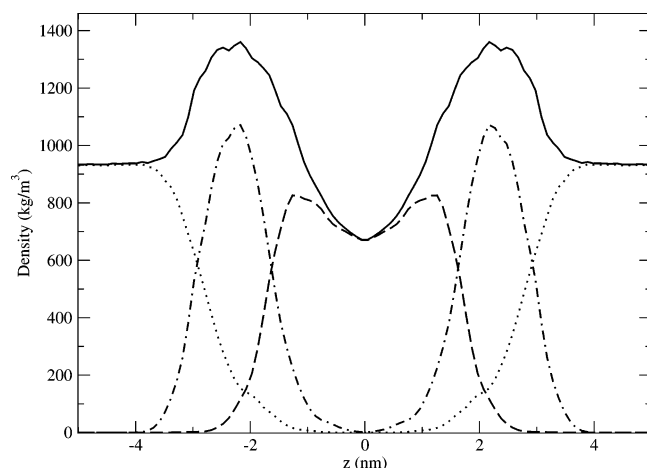


Figure 8. Mass density profile of the whole system (solid line), water (dotted line), ceramide tails (dashed line), and saccharidic headgroups (dot-dashed line). The profiles have been symmetrized with respect to the origin.

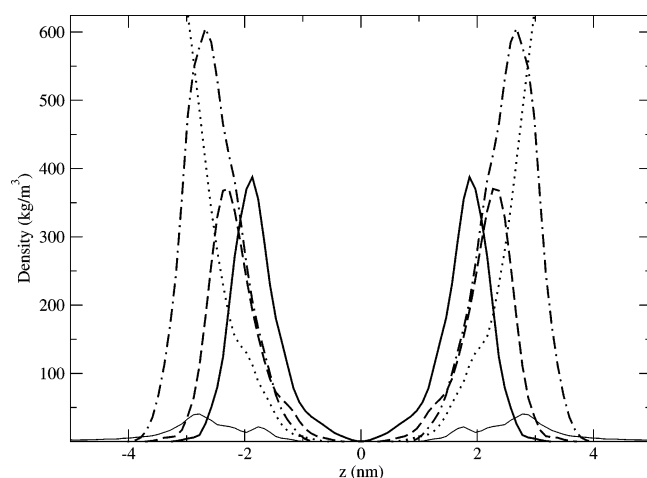


Figure 9. Mass density profile of glucose (solid line), galactose (dashed line), and sialic acid (dot-dashed line) residues, water (dotted line), and Na^+ counterions (thin solid line). The profiles have been symmetrized with respect to the origin.

The degree of chain disorder can be quantified by examining the deuterium order parameter, $S_{\text{CD}}(n)$, defined as

$$S_{\text{CD}}(n) = \frac{1}{2} \langle 3 \cos^2(\eta_n) - 1 \rangle \quad (2)$$

where η_n is the angle encompassed by the C–H bond vector of the n -th carbon with the z axis. Because of the use of united atoms, such a direction has been reconstructed by using the positions of the C_n , C_{n-1} , and C_{n+1} atoms.²⁸

The order parameter of the hydrocarbon chains, which is presented in Figure 11, is generally lower than that in phospholipid membranes (see, for example, Figure 5 in ref 10) by at least a factor of 2, thus confirming a high degree of disorder. It has to be noticed that the sphingosine's order parameter is lower than that for the fatty acid and even negative in the case of the first carbon atom. This feature can be ascribed to the presence of the double bond, since unsaturated carbon atoms are known to be responsible for a substantial reduction in the overall deuterium order parameter.²⁹ Nevertheless, in the present case, even the saturated hydrocarbon tail—the fatty acid—presents a disorder higher than that for phospholipids,¹⁰ which reflects on the relatively large steric occupancy of the carbohydrate headgroup. Actually, the mean occupied surface per head is 0.67 nm^2 , about 10% larger than that for DPPC.¹⁰ The

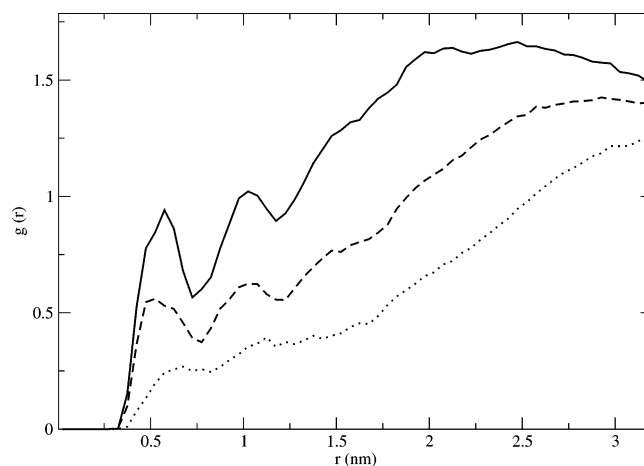


Figure 10. Radial distribution function of CH_3 with respect to the center of mass of glucose (solid line), galactose (dashed line), and sialic acid (dotted line) residues. The CH_3 coordination number is equal to 1.5, 0.9, and 0.6 for glucose, galactose, and sialic residues, respectively.

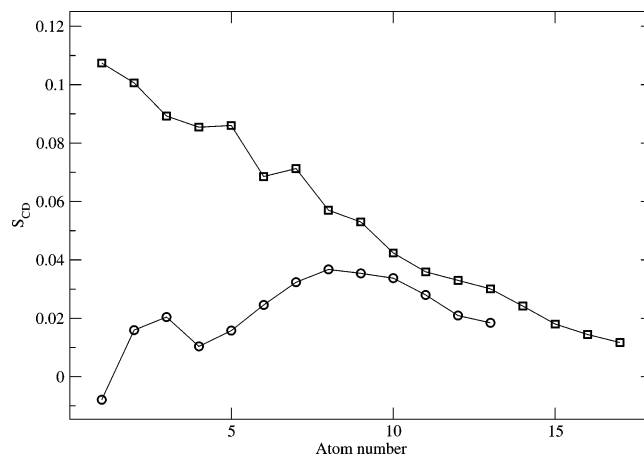


Figure 11. Deuterium order parameter of the hydrocarbon chains of the ceramide, namely, the fatty acid (squares) and the sphingosine (circles). The rightmost points in the figure are referring to the end-terminal CH_2 group. The lines are guides to the eye.

steric hindrance of the hydrophilic moiety affects the underlying hydrophobic region, where the tails tend to occupy the available lateral space, thus becoming more disordered. The high degree of disorder in the tail region confirms that at the chosen thermodynamic conditions the simulated system reproduces the L_α liquid-crystalline phase.³⁰

Turning our attention to the region of the headgroups, a clear difference between DPPC and GM3 membranes appears when the units composing the head are separately observed. In Figure 9, the mass density profiles of the three sugar units, along with that of water and Na^+ , are reported. The three sugar rings of the headgroup (i.e., sialic acid, galactose, and glucose residues) are found to have peaks at distinct positions. The same is not true for DPPC (see, for example, ref 20), where the peaks corresponding to the two charged groups are on top of each other. This is due to the fact that the charged groups composing the phospholipid head lay preferentially on the bilayer surface so as to minimize the dipole–dipole interaction energy.³⁰

The distinct positions of the peaks in GM3 are a consequence of the orientational order of the three sugar rings, which are found to be mainly aligned along the normal to the bilayer. The orientational order of the head is studied by looking at the distribution of the angles of the vectors that characterize the planes of the head rings and the direction of the rings

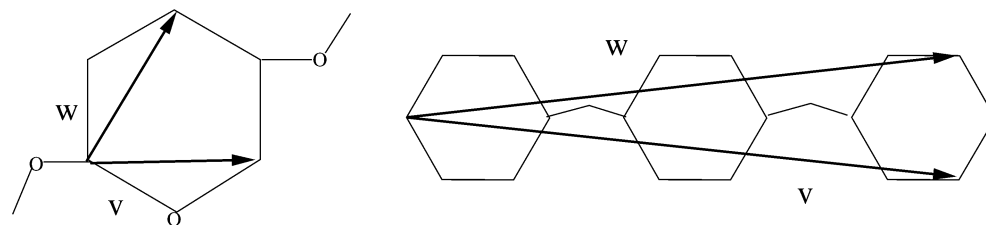


Figure 12. Schematic drawing showing the two vectors \mathbf{v} and \mathbf{w} used to define the plane of a sugar ring (left) and the whole headgroup (right). See the text for details.

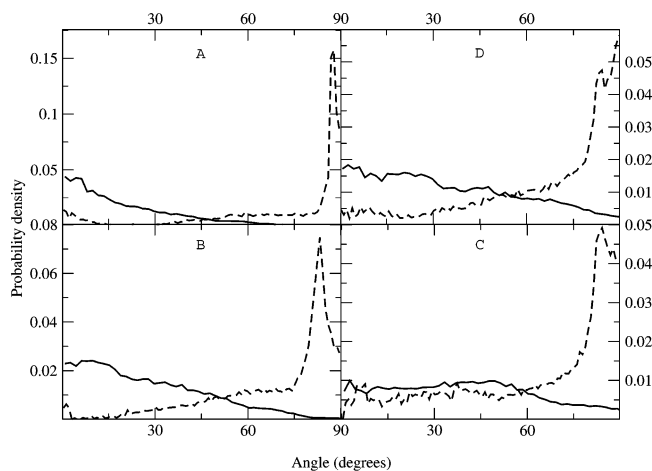


Figure 13. Normalized distributions of the orientation of the vectors \mathbf{v}_{in} (solid line) and \mathbf{v}_p (dashed line), with respect to the bilayer's normal. Panels A, B, C, and D refer to the entire headgroup and glucose, galactose, and sialic acid residues, respectively.

themselves, called θ_p and θ_{in} , respectively. By choosing two vectors, \mathbf{v} and \mathbf{w} , that characterize the sugar rings' plane, as illustrated in Figure 12, we define the vector $\mathbf{v}_{in} = (\mathbf{v} + \mathbf{w})/|\mathbf{v} + \mathbf{w}|$ to identify the longitudinal direction and the vector $\mathbf{v}_p = (\mathbf{v} \times \mathbf{w})/|\mathbf{v} \times \mathbf{w}|$ to identify the direction perpendicular to the group's plane. The directions are projected onto the unit vector perpendicular to the layer plane $\hat{\mathbf{n}}$, so that $\theta_{in} = \arccos(\mathbf{v}_{in} \cdot \hat{\mathbf{n}})$ and $\theta_p = \arccos(|\mathbf{v}_p \cdot \hat{\mathbf{n}}|)$.

Given the angular histogram, $\langle N(\theta) \rangle$, the probability distribution is given by $\psi(\theta) = \langle N(\theta) \rangle / \sin(\theta)$. The normalized probability distributions for θ_p and θ_{in} , relative to the whole headgroup and glucose, galactose, and sialic acid residues, are reported in Figure 13. For each group, the plane is found to be highly aligned with the membrane perpendicular axis, since the distribution of θ_p is peaked at 90°. Moreover, the distribution for θ_{in} has a maximum around zero degrees but is more spread out than that for θ_p , thus pointing out that the headgroups are tilted with some degree of random orientation.

The fact that the longitudinal axis of the headgroup is mostly aligned with the membrane perpendicular axis suggests that GM3 molecules present a good packing and explains why phospholipids and GM3 were found to have a similar occupied area per head. Given the large difference in the number of atoms, a naive picture would have assigned to GM3 a much larger area per head. On the other hand, the dipolar interactions drive the phospholipid heads to lay on the bilayer surface, occupying a wide surface portion. The GM3 heads do not present a strong dipolar interaction, and consequently, they align parallel to the membrane perpendicular axis, thus reducing conspicuously the occupied surface.

Direct contact with experiments can be made by comparing the small-angle X-ray scattering (SAXS) intensity data. The

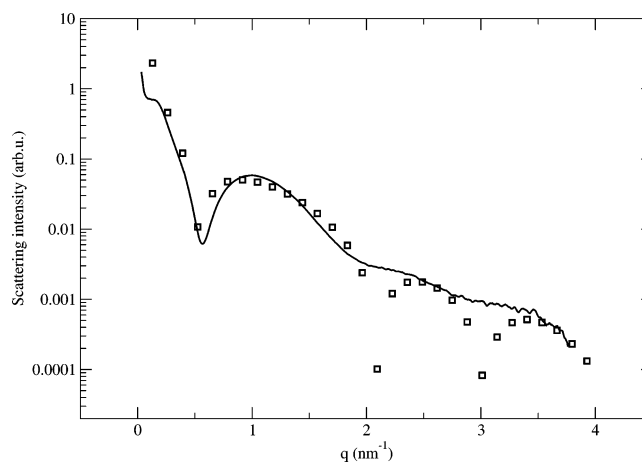


Figure 14. Scattering intensity (logarithmic scale) measured at the European Synchrotron Radiation Facility (ESRF) (solid line) and calculated from simulation (open squares) versus the modulus of the scattering vector q . The calculated data have been shifted by an arbitrary factor.

scattering intensity is computed in the limit of a diluted solution of randomly oriented bilayers via the expression

$$I(q) \propto \frac{1}{q^2} \left| \int e^{iqz} (\rho_e(z) - \rho_e^w) dz \right|^2 \quad (3)$$

where q is the modulus of the scattering vector, $\rho_e(z)$ is the electron density profile of the membrane along its normal direction, and ρ_e^w is the average electron density of bulk water. This approximation is valid only at moderately low scattering angles. In fact, it fails both at high angles—due to interatomic correlations—and at very low angles, where the global shape of the aggregate begins to be detected by the scattered radiation. SAXS data represent a valid benchmark to test the simulated GM3 against the real system, allowing one to characterize the aggregate structure, particularly as regarding the bilayer width.

To compute the spectrum from the simulation data, the average electron density profile has been extended up to 20 nm in both the positive and negative directions, to the value of the bulk water electron density. In Figure 14 the experimental SAXS¹¹ and simulated spectra are reported; the agreement is very good in the whole q range starting from $q = 0.3$ nm⁻¹. The minimum in the simulated intensity found at $q \approx 0.5$ nm⁻¹ is a direct manifestation of the bilayer width, which turns out to be in good agreement with that of the real system.

We now turn our attention to study the arrangement of both water and Na⁺ ions in the proximity of the GM3 headgroups. Water hydrates substantially the sugar rings composing the headgroup, as monitored by the radial distribution functions of water oxygen with respect to the center of mass of the three sugar rings, reported in Figure 15.

The coordination number for water is equal to 19.7, 4.5, and 2.6 for the sialic acid, galactose, and glucose residues, respec-

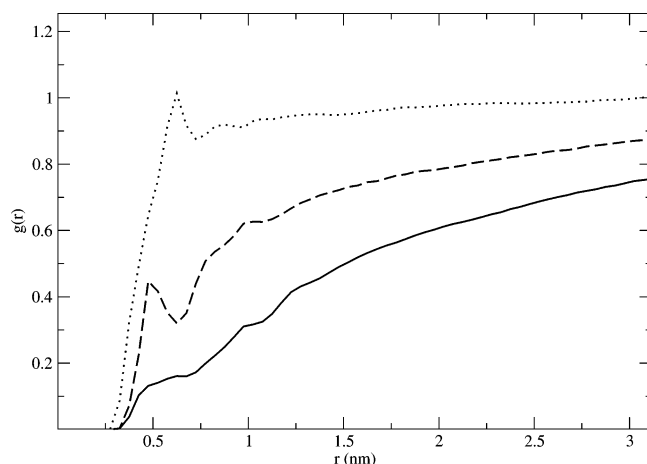


Figure 15. Radial distribution functions of water oxygen $g_{w,o}(r)$ with respect to the center of mass of glucose (solid line), galactose (dashed line), and sialic acid (dotted line) residues.

tively. For the sake of completeness, we remind the reader that in DPPC about 5.9 molecules of water are found around the phosphate group and 15.3 around the $N(\text{CH}_3)_3$ group.²⁰ Possibly, in GM3, water cannot penetrate to the level of the most buried groups of the head (glucose), since there is a significant overlap of this residue with the two hydrocarbon tails, as apparent from the density profiles shown in Figures 8 and 9.

Na^+ ions are broadly distributed and mostly located in correspondence with the sialic acid residues, that is, close to the negative charge, as expected (see Figure 9). A non-negligible percentage of ions is found to be dissolved in bulk water. It is possible to obtain the number of Na^+ ions dissolved in water by integrating the corresponding density profile and defining the region where ions are dissolved in water such that their density profile is higher than that of GM3. It is found that approximately 10% of the total number of counterions are dissolved in solution. According to the general theory for continuous media,³¹ all counterions should condensate on an infinitely wide charged bilayer. In our computer simulation, the use of periodic boundary conditions effectively models the system as a stack of infinitely wide bilayers. Moreover, one has to consider the discreteness introduced by a simulation at the molecular level, as in our case. These two facts can explain the difference in the condensed fraction of counterions on the GM3 bilayer surface.

In Figure 16 we report the radial distribution function of Na^+ ions and water around each of the oxygens of the COO^- group. The first shell coordination number obtained by integrating $g_{\text{O}^-\text{Na}^+}(r)$ up to the first minimum is 0.3, and therefore, 30% of the Na^+ ions are tightly bound to a COO^- group. The strong coordination of Na^+ ions with COO^- groups induces a $\text{Na}^+ - \text{Na}^+$ ordering. This is indicated by the well defined second peak of the Na^+ radial distribution function, which turns out to be at the same distance as that of the first peak in the $\text{O}^- - \text{O}^-$ distribution function. Moreover, the radial distribution function of water around O^- shows that Na^+ ions induce a marked coordination with the solvent.

From the charge density profiles of each molecular species, it is possible to investigate whether finite size effects are important in the simulation of GM3 bilayers. Due to the ionic character of the GM3 heads, the extent of the electrostatic interaction acting between bilayers belonging to different images of the simulated system can be significant. The profile of the electric field along the z direction is calculated by integrating

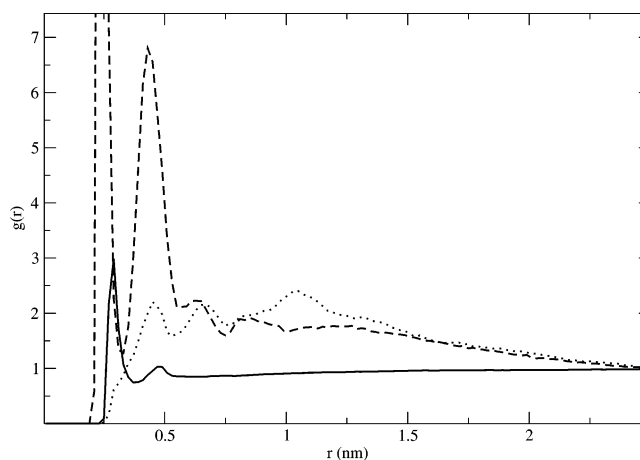


Figure 16. Radial distribution functions of the COO^- oxygen atoms with respect to the water oxygen (solid line), Na^+ ion (dashed line), and COO^- oxygen atoms belonging to distinct GM3 molecules (dotted line).

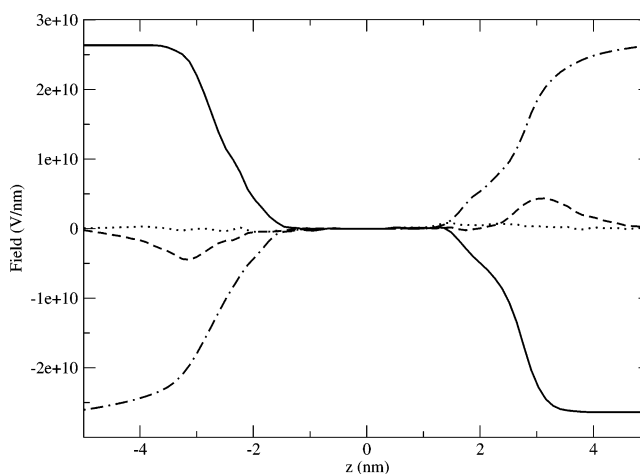


Figure 17. Contributions to the electric field arising from GM3 (solid line), water (dashed line), and Na^+ ions (dot-dashed line), as well as the total electric field (dotted line).

the charge density across the simulation box according to the expression

$$E(z) = \frac{1}{\epsilon_0} \int_{-L}^z \rho_q(z') dz' + C \quad (4)$$

where $\rho_q(z')$ is the average charge density profile, $-L$ corresponds to the midpoint between periodic replicas of the membrane, and the constant C is chosen so that the field at the center of the bilayer is zero, as it should be for an ideal system with no fluctuations in the $x-y$ plane and composed of two symmetric monolayers.²⁰

Figure 17 illustrates the profile of the electric field across the simulation box, having separated the contributions arising from different species. As apparent, the charge unbalance arises mostly from the GM3 heads and sodium. Anyway, the contribution due to water is not negligible. From the figure, it is also clear that most of the counterions condensate in the proximity of the membrane surface, while a slow decay develops away from the membrane. Water, consistently, shows a similar slowly decaying tail when approaching the bulk region. The behavior of the electric field within the water layer suggests that the electrostatic field induces a strong orientational polarization of the solvent which persists over a large region.

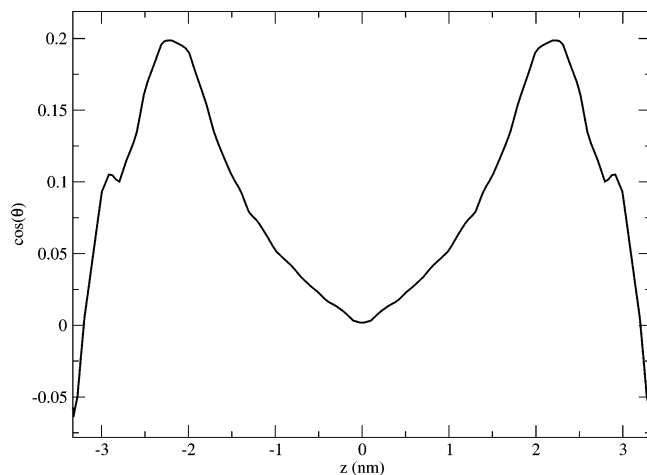


Figure 18. Orientational order parameter of water. Data have been refolded so that the origin coincides with the midpoint between periodic images of the bilayer. The figure has been symmetrized with respect to the origin.

To quantify such an effect, we looked at the orientational order of water by computing the projection of the water dipole unit vector onto the normal to the bilayer surface, $\langle \cos(\theta) \rangle$. Results are shown in Figure 18, where the profile has been refolded so that the origin coincides with the midpoint between periodic images of the membrane. The most important result is that the orientational order parameter decays rather slowly when going toward the bulk region. The parameter drops to zero at $z = 0$, as imposed by the periodic boundary conditions. The slow decay seems to be a peculiarity of the ionic nature of GM3. In fact, in the case of nonionic amphiphiles such as phospholipids, the polarization of water vanishes over an extension of about 1 nm (see, for example, Figure 3 in ref 32 and Figure 1 in ref 11). The orientational order parameter suggests that the chosen size of the system is large enough to allow for water to depolarize. However, the lack of a clear plateau cannot exclude finite size effects due to incomplete depolarization of water. Therefore, we have undertaken new simulations to investigate in greater detail such a possibility, and results will be presented elsewhere.

4. Conclusions

In this paper results of the first molecular dynamics simulation of a GM3 ganglioside bilayer at full atomistic detail have been reported. The force field adopted to model the system is a modified version of the GROMOS87 one. Namely, the carbohydrate part has been improved by using the parameters suggested by Berger, and the rigidity of the sugar rings has been accounted for by following the procedure suggested by Spieser. Very long relaxation times have been observed in bringing the system to an equilibrated configuration. In particular, the glycosidic torsional angles appear to be the slowest indicators of relaxation toward equilibrium. The quality of the simulated system was benchmarked against experimental data given by small-angle X-ray scattering. The comparison with the experimental results is particularly good, lending us to believe that the modelization of the bilayer provides a good description of the real system. Several properties have been computed and compared with those of phospholipid bilayers. Tails are found to be more disordered in GM3 than in phospholipids under similar thermodynamic conditions. As far as the orientation of the headgroups is concerned, it has been shown that the sugar

rings preferentially lay on a plane orthogonal to the bilayer surface while the head longitudinal axis presents some degree of tilting. When looking at the membrane–water interface, the hydration of the whole headgroup is more pronounced in GM3 than in phospholipids, due to the strong hydrophilic character of the GM3 headgroups. About 90% of all the Na^+ ions are found to be condensed in the headgroup region. Finally, a slowly decaying polarization of water away from the membrane has been observed, in sharp contrast to the case of phospholipids.

In conclusion, we have proved that a realistic simulation of the GM3 ganglioside bilayer is feasible on the time scale accessed by simulation. This result paves the way to more extensive studies concerning both the structural and dynamical properties of the GM3 bilayer under different thermodynamic conditions. Work in this direction is in progress.

Acknowledgment. This work has been done under the FIRB project “Study of micro systems for controlled drug delivery”, financed by the Italian Ministry of Education. We wish to thank Dr. Pal Jedlovsky for a useful reading of the manuscript and Prof. Laura Cantù for helpful discussions. Computer resources from the CINECA Supercomputing Center are kindly acknowledged.

References and Notes

- (1) Hakomori, S.; Young, W. W., Jr. *Handbook of Lipid Research. 3. Sphingolipid Biochemistry*; Plenum Publishing Corp.: New York, 1983; pp 381–436.
- (2) Masserini, M.; Ravasi, D.; Sonnino, W. *Trends Glycosci. Glyco-technol.* **2001**, *13* (71), 239–250.
- (3) Hakomori, S.-I. *J. Biol. Chem.* **1990**, *265* (31), 18713–18716.
- (4) Siebert, H.-C.; Reuter, G.; Schauer, R.; von der Lieth, C.-W.; Dabrowski, J. *Biochemistry* **1992**, *31*, 6962–6971.
- (5) Cantù, L.; Favero, E. D.; Dubois, M.; Zemb, T. N. *J. Phys. Chem.* **1998**, *B102*, 5737–5743.
- (6) Cantù, L.; Corti, M.; Favero, E. D.; Muller, E.; Raudino, A.; Sonnino, S. *Langmuir* **1999**, *15* (15), 4975–4980.
- (7) Corti, M.; Cantù, L.; Favero, E. D. *Nuovo Cimento Soc. Ital. Fis.* **1994**, *16 D*(9), 1391–1400.
- (8) Cantù, L.; Corti, M.; Favero, E. D.; Raudino, A. *J. Phys. II* **1994**, *4*, 1585.
- (9) Brocca, P.; Bernardi, A.; Raimondi, L.; Sonnino, S. *Glycoconj. J.* **2000**, *17*, 283–299.
- (10) The presented data have to be considered preliminary results. A more detailed analysis will be presented elsewhere.
- (11) Berger, O.; Edholm, O.; Jahnig, F. *Biophys. J.* **1997**, *72*, 2002–2013.
- (12) Jedlovsky, P.; Mezei, M. *J. Phys. Chem.* **2001**, *B105*, 3614–3623.
- (13) Lindahl, E.; Hess, B.; van der Spoel, D. *J. Mol. Model.* **2001**, *7*, 306–317.
- (14) Berendsen, H. J. C.; van der Spoel, D.; van Drunen, R. *Comput. Phys. Commun.* **1995**, *91*, 43–56.
- (15) Koehler, J. E. H.; Saenger, W.; van Gunsteren, W. F. *Eur. Biophys. J.* **1987**, *15*, 197–210.
- (16) Ryckaert, J. P.; Bellemans, A. *Faraday Discuss. Chem. Soc.* **1997**, *18*, 1463–1472.
- (17) Schuettelkopf, A. W.; van Aalten, D. M. F. *Acta Crystallogr.* **2004**, *D60*, 1355–1363.
- (18) Klewinghaus, P.; van Eijck, B. P.; Kouwijzer, M. L. C. E.; Kroon, J. *THEOCHEM* **1997**, *395–396*, 289–295.
- (19) Kroon-Batenburg, L. M. J.; Kruiskamp, P. H.; Vliegthart, J. F. G.; Kroon, J. *J. Phys. Chem.* **1997**, *B101*, 8454–8459.
- (20) Spieser, S. A. H.; van Kuik, J. A.; Kroon-Batenburg, L. M. J.; Kroon, J. *Carbohydr. Res.* **1999**, *322*, 264–273.
- (21) Tieleman, D.; Bernedsen, H. J. C. *J. Chem. Phys.* **1996**, *105*, 4871–4880.
- (22) Patra, M.; Karttunen, M.; Hyvonen, M.; Falck, E.; Lindqvist, P.; Vattulainen, I. *Biophys. J.* **2003**, *84*, 3636–3645.
- (23) Essman, U.; Perera, L.; Berkowitz, M. L.; Darden, T.; Lee, H.; Pedersen, L. G. *J. Chem. Phys.* **1995**, *103*, 8577–8592.
- (24) Ryckaert, J. P.; Ciccotti, G.; Bernedsen, H. J. C. *J. Comput. Phys.* **1977**, *23*, 327–341.
- (25) Miyamoto, S.; Kollman, P. A. *J. Comput. Chem.* **1992**, *13*, 952–962.

- (26) Hess, B.; Bekker, H.; Berendsen, H. J. C.; Fraaije, J. G. E. M. *J. Comput. Chem.* **1997**, *18*, 1463–1472.
- (27) Berendsen, H. J. C.; Postma, J. P. M.; DiNola, A.; Haak, J. R. *J. Chem. Phys.* **1984**, *81*, 3684–3690.
- (28) Merritt, E. A.; Bacon, D. J. *Methods Enzymol.* **1997**, *277*, 505–524.
- (29) Egberts, E.; Berendsen, H. J. C. *J. Chem. Phys.* **1988**, *89*, 3718–3732.
- (30) Saiz, L.; Klein, M. L. *Biophys. J.* **2001**, *81*, 204–216.
- (31) Egberts, E.; Marrink, S.-J.; Bernedsen, H. J. C. *Eur. Biophys. J.* **1994**, *22*, 423–436.
- (32) McLeughlin, S. *Annu. Rev. Biophys. Biophys. Chem.* **1989**, *18*, 113–136.
- (33) Åman, K.; Lindahl, E.; Edholm, O.; Håkansson, P.; Westlund, P.-O. *Biophys. J.* **2003**, *84*, 102–115.